Carbohydrate Polymers 191 (2018) 127–135

Contents lists available at ScienceDirect

Carbohydrate Polymers

journal homepage: www.elsevier.com/locate/carbpol

Chitosan functionalized poly-ε-caprolactone electrospun fibers and 3D printed scaffolds as antibacterial materials for tissue engineering applications

Myriam G. Tardajos[a], Giuseppe Cama[a], Mamoni Dash[d], Lara Misseeuw[a], Tom Gheysens[a], Christian Gorzelanny[b], Tom Coenye[c], Peter Dubruel[a,*]

[a] Polymer Chemistry & Biomaterials Research Group (PBM), Ghent University, Krijgslaan 281, S4-Bis, B-9000 Ghent, Belgium
[b] Department of Dermatology, Medical Faculty Mannheim, Heidelberg University, Theodor-Kutzer-Ufer 1-3, 68167 Mannheim, Germany
[c] Laboratory of Pharmaceutical Microbiology, Ghent University, Ottergemsesteenweg 460, 9000, Ghent, Belgium
[d] Institute of Life Sciences. Nalco Square, Bhubaneswar-751023. India

ARTICLE INFO

Keywords:
Chitosan
Surface functionalization
Scaffolds
Poly-ε-caprolactone
Antibacterial

ABSTRACT

Tissue engineering (TE) approaches often employ polymer-based scaffolds to provide support with a view to the improved regeneration of damaged tissues. The aim of this research was to develop a surface modification method for introducing chitosan as an antibacterial agent in both electrospun membranes and 3D printed poly-ε-caprolactone (PCL) scaffolds. The scaffolds were functionalized by grafting methacrylic acid *N*-hydroxysuccinimide ester (NHSMA) onto the surface after Ar-plasma/air activation. Subsequently, the newly-introduced NHS groups were used to couple with chitosan of various molecular weights (Mw). High Mw chitosan exhibited a better coverage of the surface as indicated by the higher N% detected by X-ray photoelectron spectroscopy (XPS) and the observations with either scanning electron microscopy (SEM)(for fibers) or Coomassie blue staining (for 3D-printed scaffolds). A lactate dehydrogenase assay (LDH) using L929 fibroblasts demonstrated the cell-adhesion and cell-viability capacity of the modified samples. The antibacterial properties against *S. aureus* ATCC 6538 and *S. epidermidis* ET13 revealed a slower bacterial growth rate on the surface of the chitosan modified scaffolds, regardless the chitosan Mw.

1. Introduction

Tissue engineering (TE) represents a growing multidisciplinary scientific field, where knowledge from different areas is combined in order to produce biological substitutes to restore, maintain, or improve tissue function (Chua, 2001, 2002;). One of the most effective approaches in tissue engineering involves the seeding of porous, biocompatible, biodegradable 3D scaffolds with cells with a view to promoting tissue regeneration (Achilli, Meyer, & Morgan, 2012; Worthington, Pochan, & Langhans, 2015). The basic scaffold characteristics for a successful tissue engineering outcome are a physically stable and structurally porous shape, interconnectivity, high porosity, and appropriate surface functionality. With a view to these properties, polyesters, in particular poly-ε-caprolactone (PCL), have been extensively exploited to produce scaffolds for biomaterial applications. The popularity of PCL for such applications can be attributed to its biocompatibility, biodegradability and high processability (Coombes et al., 2004; Hutmacher et al., 2001; Li et al., 2005; Si, Cui, Wang, Liu, & Liu, 2016; Woodruff & Hutmacher, 2010). However, a major limitation of PCL is its lack of functional groups, which are required for biofunctionalization in order to adapt and tailor the polymer to the specific biomedical need.

Consequently, the introduction of different functional groups on the PCL surface has been thoroughly investigated to enable subsequent (bio)polymer immobilization. For example, methacrylic acid (MA) was grafted following aminolysis with a view to facilitating subsequent collagen coupling (Yuan, Xiong, Wang, Zhang, & Choong, 2012). Other studies have realized direct covalent immobilization of chitosan, gelatin, or collagen on PCL surfaces through the introduction of NH2 groups via aminolysis using diamines. However, this method requires the use of the toxic cross-linking agent glutaraldehyde, which is best avoided in the fabrication of biomaterials for therapeutic purposes (Zhu, Gao, Liu, & Shen, 2002). Furthermore, aminolysis involves the cleavage of ester bonds, which in-turn decreases the average molecular

* Corresponding author at: Polymer Chemistry and Biomaterials Group (PBM), Ghent University, Department of Organic and Macromolecular Chemistry, Campus Sterre, S4-BIS, Krijgslaan 281, 9000 Ghent, Belgium.
E-mail address: Peter.dubruel@ugent.be (P. Dubruel).

https://doi.org/10.1016/j.carbpol.2018.02.060
Received 28 November 2017; Received in revised form 2 February 2018; Accepted 20 February 2018
Available online 21 February 2018
0144-8617/

weight of the (surface located) polyester, thus possibly compromising the mechanical integrity of the scaffolds. In order to minimize such undesirable factors, the non-thermal plasma activation of polymer surfaces has been proposed (Desmet et al., 2009; Morent, De Geyter, Desmet, Dubruel, & Leys, 2011). This technique can effectively functionalize the polyester surface without affecting its bulk properties (Ho et al., 2006). Moreover, it has the advantage of being a solvent-free technique. Our research group has previously reported on the successful immobilization of gelatin on PCL scaffolds using 2-aminoethyl methacrylate grafting after argon plasma activation (Desmet et al., 2010; Desmet, Poleunis, Delcorte, & Dubruel, 2012). Additionally, other research groups have plasma grafted acrylic acid (AA) to enable the covalent binding of collagen or laminin (Cheng & Teoh, 2004; Siri, Wadbua, Amornkitbamrung, Kampa, & Maensiri, 2010; Sousa, Mendes, Pereira, & Bártolo, 2014).

In the present study, our aim was to immobilize chitosan on PCL in a covalent manner by reacting with *N*-hydroxysuccinimide ester (NHSMA) through an argon plasma grafting activation approach (Morent et al., 2011; Suzuki, Kishida, Iwata, & Ikada, 1986). Chitosan is a biopolymer which exhibits attractive biological properties such as biocompatibility, wound healing ability, and antibacterial activity (Anitha et al., 2009; Cooper, Oldinski, Ma, Bryers, & Zhang, 2013; Doulabi, Mirzadeh, Imani, & Samadi, 2013; Feng & Xia, 2011; Martins et al., 2014; Muzzarelli et al., 1990). As chitosan lacks the desirable properties of processability and structural integrity, the application of chitosan as a coating on more rigid materials would undoubtedly open up new avenues for different TE applications, by combining the biofavorable qualities of both.

Literature details different combinations of PCL and chitosan, including blends (Ciardelli & Chiono, 2006; Mahoney, Conklin, Waterman, Sankar, & Bhattarai, 2016; Nourmohammadi, Ghaee, & Liavali, 2016; Sarasam & Madihally, 2005) and co-electrospun fibers (Ghorbani, Kaffashi, Shokrollahi, Seyedjafari, & Ardeshirylajimi, 2015; Hong & Kim, 2011; Ji, Liang, Shen, & Bowlin, 2014). A single state-of-the-art study by Chen et al. from 2014 reported on chitosan that was covalently coupled to PCL after plasma activation. In their work, oxygen plasma activation was applied. The carboxylic acids, which were introduced through the plasma activation, were used as anchoring points for the amino groups of chitosan through EDC/NHS (carbodiimide/*N*-hydroxysuccinimide) amidation chemistry (Chen, Chen, Fong, & Chen, 2014).

In the herein proposed route the NHSMA grafting, which to the best of our knowledge has not been performed before on polyesters, avoids the common side reaction that results in the formation of anhydrides instead of succinimidyl esters, as described by other authors when using EDC/NHS chemistry (Wang, Yan, Liu, Zhou, & Xiao, 2011). Moreover, the proposed grafting process increases the number of reactive points on the surface and thus its accessibility, as each of the grafted chain monomers becomes a potential anchoring point for chitosan. Finally, we investigated the influence of chitosan molecular weight on the covalent functionalization by evaluating three different types of chitosan of high, medium, and low molecular weight.

The proposed approach offers a general modification procedure that should be valid for different types of scaffolds like electrospun fiber mats and 3D printed scaffolds, both with high potential for TE applications (Bhardwaj & Kundu, 2010; Cai et al., 2013; Chia & Wu, 2015; Hockaday et al., 2012; Hollister, 2005; Peltola, Melchels, Grijpma, & Kellomäki, 2008; Pham, Sharma, & Mikos, 2006; Tan, Hu, Huang, Han, & Hu, 2015; Yen, Chen, Huang, Kuo, & Lin, 2016).

Finally, we aim to develop a new surface modification method on electrospun and 3D printed PCL scaffolds by grafting NHSMA onto the surface after Ar-plasma/air activation, to subsequently react the introduced NHS groups with chitosan as potential anti-bacterial materials.

2. Materials and methods

2.1. Materials

Poly-ε-caprolactone (PCL) pellets (Mw 80.000 g mol^{-1}, Sigma–Aldrich), methacrylic acid *N*-hydroxysuccinimide ester (NHSMA) Sigma–Aldrich, 2-(*N*-morpholino) ethanesulfonic salt (MES, Sigma–Aldrich), chloroform (Sigma–Aldrich), acetone (Sigma–Aldrich), dimethylsulfoxide (Sigma–Aldrich), were all used as received. High molecular weight chitosan (CSH, Mw 184.000 g mol^{-1} DDA 89%,) was provided by Gillet Chitosan, medium molecular weight chitosan (CSM, Mw 76.000 g mol^{-1} DDA 83%) was from Sigma–Aldrich, and low molecular weight chitosan (CSL, Mw < 5.000 g mol^{-1} DDA > 75%) was provided by Heppe Medical Chitosan. The molecular weight (Mw) and degree of deacetylation (DDA) of the chitosan products were measured by the group of Prof. Moerschbacher of Munster University, Germany. Cytotoxicity was evaluated with a LDH kit (Roche, Mannheim, Germany). The dyes used for fluorescence microscopy were, Rhodamin conjugated phalloidin (Life Technologies GmbH, Darmstadt, Germany) and 4′, 6-Diamidin-2-phenylindol (DAPI; Sigma-Aldrich GmbH, Steinheim, Germany). Coverslips were mounted in DABCO-Mowiol (Sigma-Aldrich GmbH, Steinheim, Germany).

2.2. PCL processing into fiber mats or 3D plotted scaffolds

2.2.1. Electrospun fibers

PCL fibers were prepared from a 20% (w/v) PCL solution in a 2:1 chloroform/acetone solvent mixture and placed in a 5 mL syringe. A 22-gauge needle was used for the spinning process. The distance from the needle to the collector was fixed to 15 cm and the high voltage power supply was set in the range of a 14–16 kV difference between the needle tip and the grounded collector (aluminum foil). The flow rate was set to 0.5 mL h^{-1}. Electrospinning was performed for 1.5 h at room temperature. Afterwards, sample discs with a thickness of 12.2 ± 3.11 µm were cut with an 8 mm diameter puncher from the electrospun mat. Average fiber diameter measurements were performed by analyzing three samples with six measurements per sample using scanning electron microscopy (SEM) imaging. For this purpose, the dry scaffolds were coated with a (approximately) 20 nm thin gold layer. SEM images were recorded using a tabletop SEM (PHENOM, FEI Company).

2.2.2. 3D plotted scaffolds

Porous cubic-shaped PCL scaffolds (10 × 9 × 3 mm^3) were fabricated using a Bioscaffolder® (Sys-Eng, Germany) device. The scaffolds were designed in Inventor while PrimCam (Sys-Eng, Germany) was used to create the final structure. The plotting process was performed by melting PCL pellets at a temperature of 120 °C for 1 h. The melted polymer was extruded through a 27-gauge needle at a pressure of 5 bar at 240 mm/min using a lay-down pattern of 0/90°. A Zeiss light microscope (Zeiss, Germany), in combination with an Axiovision digital camera, was used to measure the strut diameter and the pore size based on three samples and six measurements per sample. Image processing was performed using Zeiss AxioCam software (Zeiss, Germany).

2.3. Surface grafting of NHSMA and chitosan immobilization on the PCL fibers and 3D printed scaffolds

2.3.1. PCL surface plasma activation

The PCL scaffolds obtained by ES or 3D printing were activated using Argon plasma in a cylindrical dielectrical discharge plasma reactor (Model Femto, version 3, Diener Electronic, Germany). The scaffolds were subjected to surface activation for three different time points: 15, 30 and 60 s. The argon pressure was maintained at 0.8 mbar and the applied power was set to 100 W. Then, the samples were exposed to the ambient atmosphere for 5 min.

2.3.2. Grafting of NHSMA via photopolymerization

The plasma activated samples were introduced into a DMSO solution of NHSMA and irradiated in a UV device equipped with eight UV-lamps (Sylvania, F15W/350, λ_{max} = 350 nm) for 30 min. Four lamps were situated on each side of the scaffold. The grafting was achieved using a NHSMA concentration of 0.5 or 1 M. The distance between the PCL scaffolds and the lamps was set to 10 cm, resulting in an intensity of 4–5 mW cm^{-2}. After grafting, the samples were thoroughly rinsed with DMSO and subsequently reacted with chitosan as described below.

Prior to the chitosan immobilization, a rheological viscosity evaluation of the chitosan solutions, CSH, CSM, and CSL, was performed at 20 °C at a variable shear rate (10–50 s^{-1}) using a Physica MCR 350 (Anton Paar) with plate–plate geometry (25 mm diameter). Rheoplus software was used to analyze the results. The viscosity of the different chitosan solutions in 0.1 M MES buffer, pH 5 reaction conditions at 0.5 and 1 w/v% was studied to enable selection of the optimal concentration conditions.

2.3.3. Chitosan immobilization on polyNHSMA (PNHSMA)-activated PCL

The PNHSMA-grafted samples were reacted overnight under shaking in 2 mL of a 0.5–1% w/v chitosan solution in 0.1 M MES buffer at pH 5 (Chen et al., 2014). Although the optimum pH-range for NHS-ester coupling is in the pH 8.0–9.0 range, the reaction was performed at pH 5 due to the limited solubility of chitosan in more elevated pH conditions. With a view to investigating the influence of chitosan molecular weight (Mw) on the success of its immobilization, the coupling was performed using three different molecular weight chitosan products: high (CSH), medium (CSM), and low molecular weight (CSL). The degree of deacetylation (DDA) was higher than 75% for the three types of chitosan to favor the coupling reaction with the grafted PNHSMA chains. After the reaction was complete, the samples were washed with pH 2 MilliQ water for 2 h and subsequently in pH 7 MilliQ water for 2 h. Finally, the samples were dried at room temperature and stored in a desiccator. As negative controls, plasma treated non NHSMA-grafted samples were also incubated in chitosan.

After chitosan immobilization, SEM imaging was performed to visualize the chitosan surface modified fibers. For the 3D printed scaffolds a Coomassie blue staining test was performed to appreciably visualize the surface modification. In this test, the 3D printed scaffolds were incubated for 30 min in a 1:20 ethanol/MilliQ water solution with 0.05% w/v Coomassie solution, 40% v/v methanol and 10% v/v acetic acid at room temperature. Afterwards, the samples were washed (3 times) in a MilliQ solution with 40% v/v methanol and 10% v/v acetic acid for 1.5 h. In this procedure, the dye reacts with the chitosan amino groups and therefore the blue coloration gives a qualitative visual indication of the chitosan present on the surface of the 3D printed scaffolds.

2.3.4. Applied surface characterization techniques

Fourier transform infrared spectroscopy (FTIR) was performed on a Bio-Rad FTIR spectrometer FTS 575C with a resolution of 45 cm^{-1} operating in attenuated total reflection mode. The recorded spectra were analyzed using WIN-IR Pro software.

X-ray photoelectron spectroscopy (XPS) measurements were performed with an ESCA S-probe VG monochromatised spectrometer, equipped with an Al Ka X-ray source (1486 eV). Survey scans were recorded on three spots of three different samples. The elemental composition of the surface was determined by calculating the peak areas in the obtained spectra with CasaXPS software.

2.4. In vitro biocompatibility test

Prior to use, the electrospun fiber mats (diameter 8 mm, thickness 12.2 ± 3.11 μm) and 3D printed structures (10 × 9 × 3 mm^3) were sterilized in a cold ethylene oxide cycle (38 °C/aeration 48 h) in AZ Sint Jan, Brugge. L929 cells were maintained in RPMI 1640 medium supplemented with 10% fetal calf serum (FCS), 1% L-glutamine and 1% penicillin/streptomycin at 37 °C and 5% CO_2. To test the cytotoxicity of the scaffolds (4 samples per scaffold type), LDH assays were performed as previously reported (Bauer et al., 2011). Briefly, 5.0 × 104 L929 cells were seeded per scaffold and cultivated for 24 h. Supernatants were collected and the LDH activity was measured using a corresponding cytotoxicity kit.

2.4.1. Structure illumination fluorescence microscopy

The morphology of the L929 cells was analyzed by structure illumination fluorescence microscopy (SIFM) after 7 days of continuous culture. Prior to the staining, cells were fixed at 4 °C for 30 min in HEPES-buffered Ringer's solution (10 mM HEPES, 5 mM glucose, 1 mM $CaCl_2$, 1 mM $MgCl_2$,5 mM KCl, 140 mM NaCl) containing 4% paraformaldehyde. Cell membranes were permeabilized by 0.1% Triton X-100 dissolved in incubation buffer (HEPES-buffered Ringer's solution, 0.1% bovine serum albumin). Nonspecific antibody binding was blocked with incubation buffer supplemented with 2% bovine serum albumin. Cellular F-actin was stained with Rhodamin conjugated phalloidin. Nuclei were stained with 500 ng/ml 4′, 6-Diamidin-2-phenylindol (DAPI). Coverslips were mounted in DABCO-Mowiol and analyzed by SIFM using an inverted fluorescence microscope (AxioObserver.Z1, Zeiss, Jena, Germany), equipped with a structured illumination module. Images were processed and analyzed with Zen software (Zeiss, Jena, Germany).

2.5. Antibacterial assays

Staphylococcus aureus ATCC 6538 and *Staphylococcus epidermidis* ET13 biofilms were grown on the electrospun (diameter 8 mm, thickness 12.2 ± 3.11 μm) and 3D plotted (10 × 9 × 3 mm^3) sterilized samples (4 samples per type of scaffold) in the wells of a 24-well microtiter plate (TPP), using Tryptic Soy Agar (TSA, Oxoid) as the growth medium. An inoculum (200 μL) of 3.8 × 107 CFU/mL was used. After adding the cell suspensions, the plates were incubated at 37 °C for one hour to allow for adhesion. Subsequently, the bacterial suspensions were removed and the samples were rinsed with 0.9% (w/v) NaCl. After rinsing, 200 μL of fresh growth medium was added and the plates were incubated for an additional 24 h. Sessile cells were removed from the samples by three cycles of vortexing (30 s) and sonication (30 s; Branson 3510; Branson Ultrasonics Corp., Danbury, CT), and the number of CFUs/sample were determined by plating dilutions of the resulting suspensions in TSA medium (Deng et al., 2015).

The effect of the chitosan modification on surface colonization can be estimated by using Eqs. (1) and (2):

$$RI = (CFU\ 24\,h - CFU\ 1\,h)/CFU\ 1\,h, \quad (1)$$

where RI is the relative increase and CFU 1 h and CFU 24 h are the number of colony forming units recovered at 1 h and 24 h, respectively.

$$\%\ relative\ growth = (RIcs/RIpcl) \times 100, \quad (2)$$

where RIcs is the relative increase for chitosan modified samples and RIpcl is the relative increase for native PCL scaffolds.

3. Results and discussion

In the present work, PCL electrospun fiber mats (Fib-PCL) and PCL 3D plotted structures (3D-PCL) were prepared and surface modified by grafting NHSMA. Afterwards, the different molecular weight chitosans (CSH, CSM, CSL) were reacted with the grafted chains.

3.1. PCL processing

The inherent properties of PCL, such as its low melting point of around 60 °C and a glass transition temperature of about −60 °C, makes

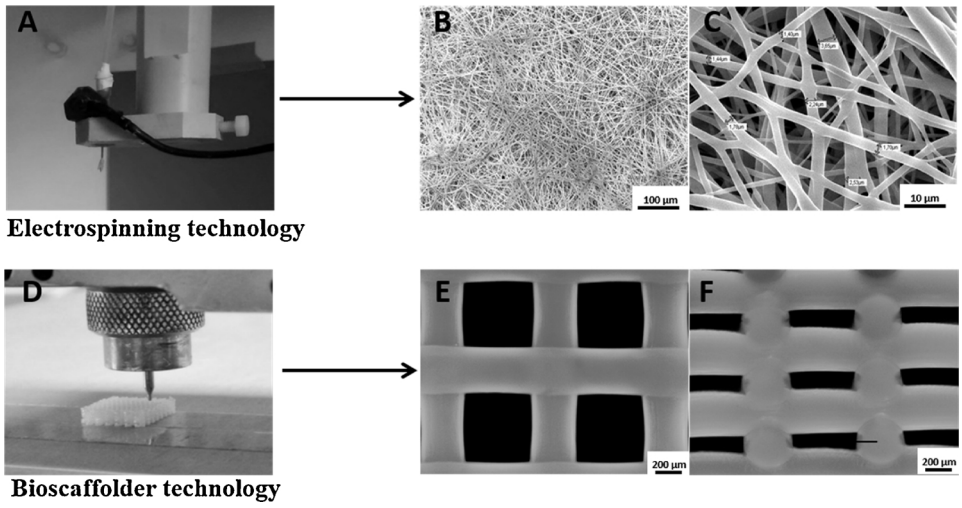

Fig. 1. Electrospinning device spinning a PCL solution (A), SEM micrograph of the electrospun PCL fibers mats with the overview of the mat (200×) (B) and a detailed zone with the fiber diameters highlighted (2500×) (C). Bioscaffolder device printing a 3D scaffold obtained by extruding melted PCL (D), Optical image (50×) of the top view of a PCL plotted scaffold detailing the porosity and the pore shape in a frontal view of the top strut layer (E), Optical image (50×) of a cross-sectional view of a PCL plotted scaffold, showing the strut diameter and evidencing the planarity of the plotted layers (F).

it easily processable and allows for scaffold design using both 3D printing and electrospinning techniques. PCL fibers were spun from a 20% (w/v) PCL solution in a 2:1 chloroform/acetone solvent mixture. Discs of 8 mm diameter and thickness of 12.2 ± 3.11 µm were cut from the electrospun mat. SEM confirmed the preparation of bead-free electrospun PCL fibers with an average diameter of 2.10 ± 0.79 µm (Fig. 1). 3D printed scaffolds were obtained with a cubic shape plotted with a 0/90 lay-down pattern scaffold. They were produced by sequential strand deposition using rapid prototyping techniques with a Bioplotter pneumatic dispensing system. Fig. 1 shows optical images of a top view and a cross section of a PCL scaffold. The average value of the scaffold strut diameter was 277 ± 14 µm. The scaffolds had square shaped pores with an average width of 440 ± 16 µm and a height of 120 ± 5 µm.

3.2. Surface modification of the electrospun and 3D printed PCL scaffolds

We sought to modify the PCL scaffolds with chitosan with a view to combining the favorable properties of both materials, including the favorable mechanical properties and processability of PCL and the hydrophilic and antibacterial properties of chitosan. The introduction of functional groups on the PCL surface was performed to enable subsequent chitosan coupling. The surface modification was done according to the scheme shown in Fig. 2. To introduce chitosan-reactive functionalities on PCL, NHSMA was grafted onto the PCL scaffolds after Ar plasma activation. Argon plasma treatment followed by air exposure of the formed radicals created peroxide groups on the surface of the PCL, a phenomenon that has been investigated and reported by our group and others previously (Cheng & Teoh, 2004; Desmet et al., 2010; Suzuki et al., 1986). These peroxides were used as initiators for the radical photopolymerization of NHSMA. The polymeric active esters introduced on the surface of the PCL scaffolds contain *N*-hydroxysuccinimide (NHS) groups. NHS is a highly reactive group that allows for the post-processing modification of the PCL structures with any (macro)molecule that contains an amino group in its structure. In the present work, NHS was used for coupling chitosan of different molecular weights via the grafted PNHSMA chains on the PCL structures. The reaction is established via the amines of the deacetylated chitosan units and the NHS groups, leading to the formation of a covalent bond between the chitosan and the PCL via an amide. This covalent bond ensures the attachment of the hydrophobic PCL to the hydrophilic chitosan.

3.3. Optimization and characterization of the surface modification

The following processing parameters involved in the modification strategy were optimized: plasma exposure time, NHSMA concentration and chitosan concentration. NHSMA was grafted using DMSO as the solvent and the UV exposure time was fixed to 30 min, owing to the limitation of the PCL solubility in DMSO. All the optimizations were performed on PCL fiber mats (Fib-PCL) and are detailed in this main text, due to the higher relative surface area and consequent higher sensitivity to conditional variations. Moreover, the impact of possible conditional variations on the 3D printed scaffolds was also studied (information available in the supporting information, SI, Table S2).

Plasma treatment time and NHSMA concentration were optimized based on X-ray photoelectron spectroscopy (XPS) analysis of the modified surfaces. The optimization was based on quantification of the extent of the grafting based on the atomic nitrogen percentage detected. All XPS spectra showed two separated peaks corresponding to C1s (286 eV) and O1s (534 eV). The detection of the nitrogen peak at 400 eV confirmed the presence of the NHS group belonging to the grafted PNHSMA chains on the Fib-PCL surface (a sample spectrum can be found in the SI, Fig. S1).

The selection of appropriate plasma activation time was a compromise between a preference for a minimal irradiation time and enabling the formation of a critical amount of radicals on the surface (Cheng & Teoh, 2004). Thus, according to the results summarized in Table S1 (SI), the selected plasma time was 30 s, as the nitrogen percentage detected was comparable to 60 s, but higher than the 15 s plasma treatment. Comparison of the atomic nitrogen percentages values (Table S1) for the NHSMA grafted samples at different NHSMA concentrations after 30 s of plasma treatment indicated a non-significant increase in the amount of PNHSMA at higher NHSMA concentrations. This implies that 0.5 M was sufficient to graft NHSMA on the Fib-PCL surface. When no UV radiation was applied on plasma treated samples incubated in 0.5 M NHSMA, no nitrogen was detected on the surface. This result confirms the absence of (P)NHSMA adsorption on Fib-PCL. The nitrogen percentage detected on the surface at the optimized plasma time and NHSMA concentration was 4.15% in the case of fiber mats, and 3.60% for the 3D printed structures (as reported in Table 1). The higher N% recorded for the fiber mats is most likely related to the higher comparative surface area available for surface modification.

After NHSMA grafting, the samples were reacted with chitosan to enable biopolymer immobilization to the PCL surface. In the present work, three types of chitosan with different molecular weights (CSH, CSM and CSL) were used.

In order to optimize the experimental concentration conditions, the viscosities of the different chitosan types were assessed through rheology. The results are reported in Fig. S2 (SI). The three chitosans were studied at 1 and 0.5% w/v concentrations in 0.1 M MES buffer, pH

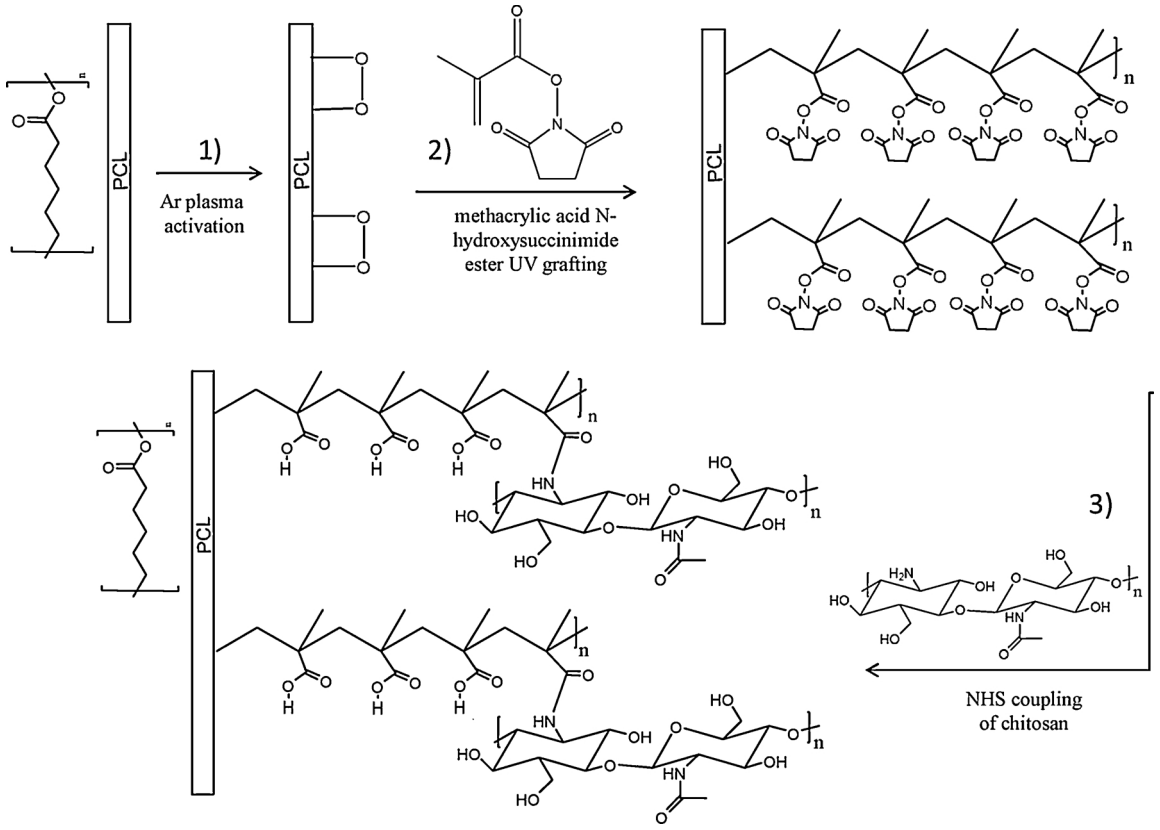

Fig. 2. Scheme of the surface modification strategy: 1) Ar plasma activation of the PCL scaffolds; 2) UV photopolymerization of NHSMA onto the plasma activated PCL surface; 3) chitosan binding by NHS coupling with the grafted chains.

Table 1
XPS analysis of surface composition of PCL fibers and 3D printed structures prior and post functionalization with NHSMA and different chitosans (CSH, CSM and CSL).

Sample	C%	O%	N%	N/C
CSH	60.71 ± 0.34	31.42 ± 0.38	7.87 ± 0.61	0.13
Fiber mats				
Fib-PCL	72.03 ± 0.43	27.97 ± 0.43	–	–
Fib-PCL-NHSMA	67.28 ± 1.39	28.57 ± 0.09	4.15 ± 1.43	0.06
Fib-PCL-CSH	64.24 ± 1.40	30.15 ± 0.37	5.59 ± 0.83 [a,b,c]	0.09
Fib-PCL-CSH-Ads	67.44 ± 0.54	29.96 ± 0.14	2.59 ± 0.46 [a]	0.04
Fib-PCL-CSM	66.89 ± 0.22	29.51 ± 0.21	3.59 ± 0.28 [b,d]	0.05
Fib-PCL-CSM-Ads	69.90 ± 0.08	27.68 ± 0.44	2.42 ± 0.51 [d]	0.03
Fib-PCL-CSL	67.14 ± 1.23	29.96 ± 0.53	2.89 ± 0.90 [c]	0.04
Fib-PCL-CSL-Ads	73.52 ± 0.41	24.82 ± 0.18	1.63 ± 0.63	0.02
3D structures				
3D-PCL	76.49 ± 1.58	23.51 ± 1.58	–	–
3D-PCL-NHSMA	69.65 ± 0.63	26.56 ± 0.25	3.60 ± 0.13	0.06
3D-PCL-CSH	66.75 ± 0.92	28.48 ± 0.52	4.77 ± 0.7 [e,f,g]	0.07
3D-PCL-CSH-Ads	73.29 ± 0.13	25.38 ± 0.54	1.32 ± 0.4 [e]	0.02
3D-PCL-CSM	67.90 ± 1.08	28.79 ± 0.90	3.31 ± 0.42 [f,h]	0.05
3D-PCL-CSM-Ads	74.19 ± 0.96	24.13 ± 0.78	1.68 ± 0.18 [h]	0.02
3D-PCL-CSL	69.17 ± 0.83	27.60 ± 0.40	3.22 ± 0.5 [g]	0.05
3D-PCL-CSL-Ads	73.98 ± 2.37	24.52 ± 0.25	1.49 ± 2.11	0.02

Samples which are significantly different under the t-student test are marked with the same letter (a,b,c,…, h) ($p < 0.05$).

5. CSM and CSL showed low viscosity and Newtonian fluid behavior at both concentrations, meaning a constant viscosity with shear change. However, CSH exhibited much higher viscosity, which was dependent on the shear rate at 1% w/v. Based on these observations, the experimental conditions selected were CSM and CSL at 1% w/v and CSH at 0.5% w/v, to work at the highest concentrations possible while retaining low viscosity to favor the reaction with the PNHSMA-grafted PCL scaffolds.

In summary, the following parameters were selected for the surface modification procedure: 30 s Ar-plasma activation time, 0.5 M NHSMA concentration in DMSO solution, 30 min UV photopolymerization exposure time and chitosan concentrations of 0.5% w/v for CSH and 1% w/v for CSM and CSL.

The success of the chitosan surface modification route followed was quantitatively evaluated by XPS analysis. The atomic percentages of carbon, oxygen, and nitrogen obtained for both types of scaffolds, electrospun fibers and 3D printed structures are shown in Table 1. The data of the atomic composition of chitosan (CSH) was used as a reference indicator of the homogeneity of the chitosan coverage on the scaffolds. In the case of chitosan, a N/C ratio of 0.13 was detected. The unmodified scaffolds (Fib-PCL and 3D-PCL) showed, as expected, only two peaks corresponding to carbon and oxygen.

The nitrogen detected on the XPS spectra could only be assigned to chitosan chains as the reaction conditions (overnight 0.1 M MES buffer pH 5) would have hydrolyzed the unreacted NHS. Nevertheless, grafted samples were incubated in the reaction conditions in the absence of chitosan as a negative control and no nitrogen was detected on the XPS measurements, as expected. Based on the results detailed in Table 1, it is possible to conclude that the covalent chitosan coupling was successful in all cases, confirmed by the detection of the nitrogen peak. For PCL fibers, fibers modified with high molecular weight chitosan, Fib-PCL-CSH showed a N/C ratio (0.09) similar to the reference chitosan (0.13). When analyzing the results obtained in the reaction with medium molecular weight (Fib-PCL-CSM) and low molecular weight chitosans (Fib-PCL-CSL), a lower N/C ratio (0.05 and 0.04, respectively) compared to CSH was detected. This indicated more efficient chitosan immobilization in the case of CSH and suggested more homogenous coverage over the sample surface. Moreover, the differences in surface modification between CSM and CSL based on the N/C ratios detected was not significant (see Table 1). Accordingly, the subsequent biological evaluation of the scaffolds was only performed on

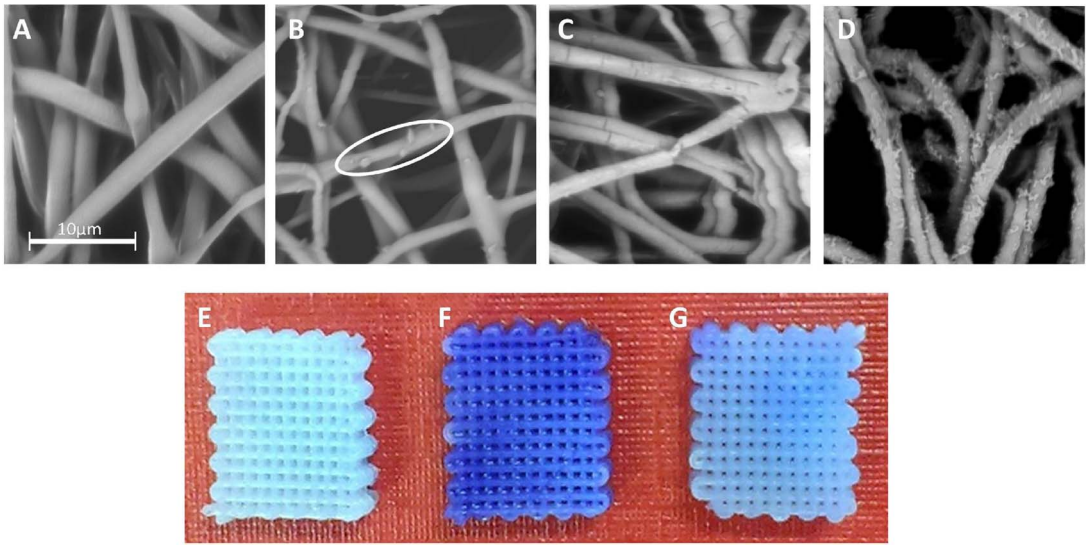

Fig. 3. Top: SEM micrographs of PCL fibers (A), Fib-PCL-NHSMA (B) (the circle shows some of the isles observed as example), Fib-PCL-CSH (C) and Fib-PCL-CSL (D). Scale bar plotted in micrograph A correspond also to B, C and D. Bottom: Picture of 3D printed structures on PCL subjected to a Coomassie staining test on (E), 3D-PCL-CSH (F), and 3D-PCL-CSL (G).

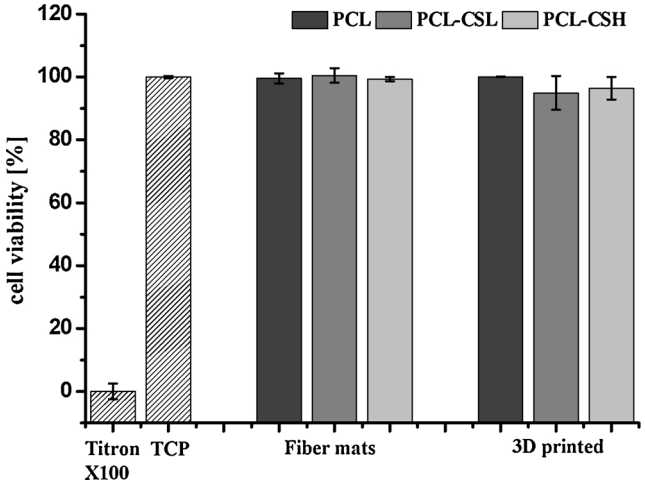

Fig. 4. Cell viability results using fibroblasts (L929 cells) grown on chitosan (CSH or CSL) modified samples and native PCL structures. Cell viability was related to the amount of released lactate dehydrogenase (LDH) measured 24 h after seeding the cells. Cells treated with 0.1% triton X-100 served as the negative controls (0% viability). Cells cultivated on tissue-culture treated polystyrene were used as the positive controls and were set to 100% viability (Gorzelanny et al., 2016; Mendes, Gorzelanny, Halter, Schneider, & Chronakis, 2016).

samples modified with CSH and CSL to analyze the possible influence of the molecular weight on the biological properties.

To confirm that the observed nitrogen signal on the chitosan reacted samples was coming from effective coupling with the grafted chain NHS groups, and was not only due to adsorption of chitosan on the surface, equivalent samples were prepared without NHSMA grafting as negative controls. The XPS data of these samples, where chitosan would be adsorbed ("ads" suffix in the table), showed that some adsorption was taking place as evidenced from nitrogen detection. Nonetheless, the N/C ratio on the pre-grafted samples was significantly higher, and therefore the chitosan detected on the surface modified samples was mainly due to covalently bonded chitosan.

Analogous conclusions were obtained from the data of the modified 3D printed scaffolds in terms of the different steps of the surface functionalization and the chitosan used. Nevertheless, when comparing the results of surface modification on fibers and 3D scaffolds, the functionalization appeared to be more effective on the fibers. In fact, a higher N/C ratio (0.09) was measured for CSH bound fibers in comparison to 3D printed scaffolds (0.07). As already mentioned, the higher surface area of the fibers most likely facilitated the reaction, which might explain the observed difference. Moreover, for the same reason, the 3D printed scaffolds were less likely to show chitosan adsorption as shown in Table 1 (N% detected lower than 1.7).

The chemical changes on the surface after each step of the modification were also followed by FTIR spectroscopy (Fig. S3). The spectra of the reference materials PCL and CSH were recorded. For pure PCL scaffolds, the ester stretching of PCL at 1720 cm^{-1} was observed as the major peak in the spectra. In the case of chitosan (CSH), the characteristic bands were in the region of 2800–3500 cm^{-1}, arising from the stretching of the OH groups and the C—H bonds. Other relevant bands for chitosan, at 1650 cm^{-1} and 1591 cm^{-1} were assigned to the stretching vibration of the C—N together with the C═O and the N—H, respectively. The spectra of the PNHSMA grafted PCL scaffolds showed two weak bands at 1807 cm^{-1} and 1770 cm^{-1} next to the ester stretching of PCL. These bands correspond to the vibrations of the NHS group (Lee, Lee, & Schmidt, 2008). After reaction of the NHS groups with chitosan, the IR spectra showed the ester stretching of PCL, but the bands corresponding to NHS were no longer present. Moreover, all the characteristic bands for chitosan were found in the PCL-CSH spectra, confirming the presence of chitosan on the surface of the PCL scaffolds. When trying to determine the changes in the surface hydrophilicity by Static contact angle (SCA) measurements before and after modification, only data could be obtained from unmodified scaffolds. After modification, the water drops were immediately taken up in the mats indicating a clear increase of the hydrophilic properties of the modified surface making it impossible to measure.

The observations from the SEM analysis supported the results obtained from the XPS and FTIR measurements in the case of the fiber mats (Fig. 3). Micrograph B of Fig. 3 shows that the grafting process of NHSMA created isles on the surface of the fibers. CSM and CSL led to inhomogeneous chitosan binding as shown in micrograph D (only one picture is included in the figure as no differences between these chitosans were observed). On the other hand, CSH effectively reacted with the electrospun fibers in a homogeneous manner resulting in complete coverage of the fiber surface (micrograph C). These results agreed with the XPS analysis where a N/C ratio close to that of the chitosan reference was detected for the modification performed with CSH.

In the case of 3D printed scaffolds, neither SEM nor optical microscopy gave any relevant information. Therefore, a colorimetric qualitative test based on Coomassie blue staining was applied to them. This test detects free amines on the surface of the scaffolds as they react with

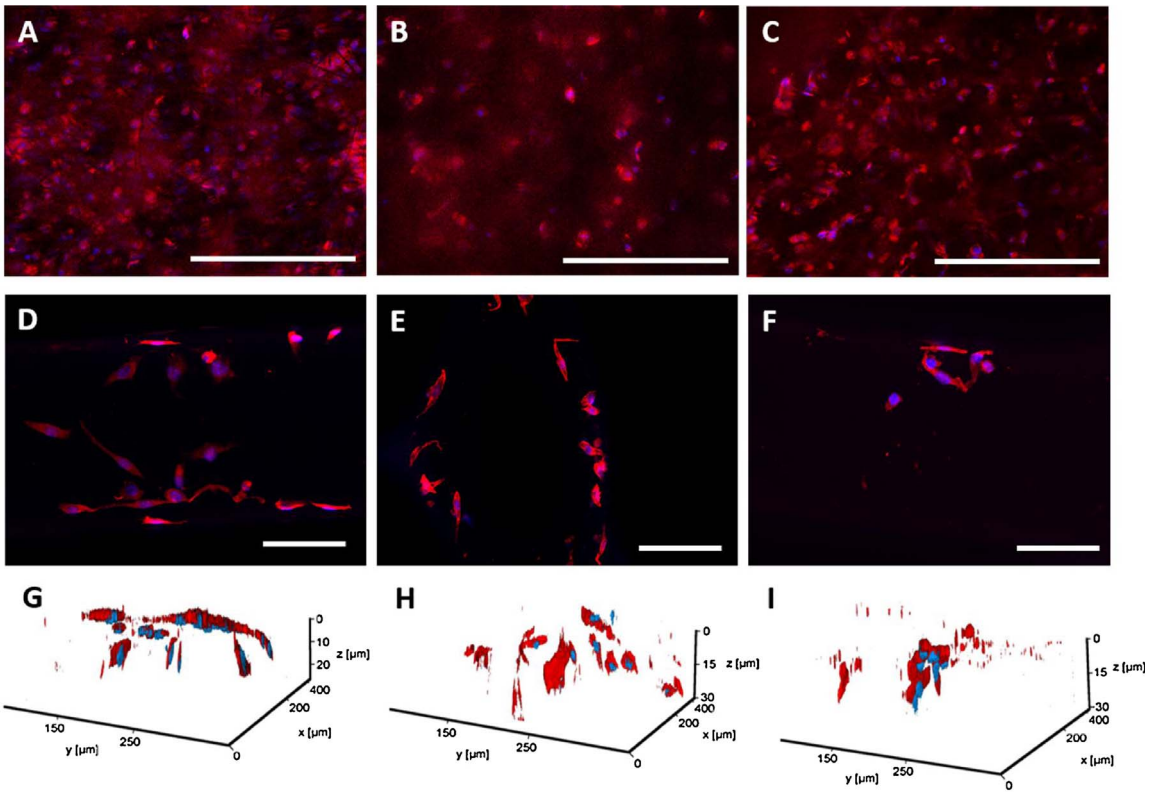

Fig. 5. Structured illumination fluorescence micrographs of fibroblasts (L929 cells) grown on chitosan (CSH or CSL) modified samples and native PCL structures. L929 cells were cultivated for 7 days either on electrospun fiber mats (Fib-PCL (A), Fib-PCL-CSH (B), Fib-PCL-CSL (C)) or on 3D printed structures (3D-PCL (D, G), 3D-PCL-CSH (E, H) and 3D-PCL-CSL (F, I)). The first two rows show maximum intensity images calculated from corresponding z-stacks. White scale bars correspond to 100 µm. Three-dimensional views of cells grown on 3D printed structures are shown in the bottom row, detailing the presence of the cells at different height levels predetermined by the printed scaffold. Cell bodies were visualized through the staining of f-actin using Rhodamin-labeled phalloidin (red). Cell nuclei were stained with DAPI (blue). (For interpretation of the references to colour in this figure legend, the reader is referred to the web version of this article.)

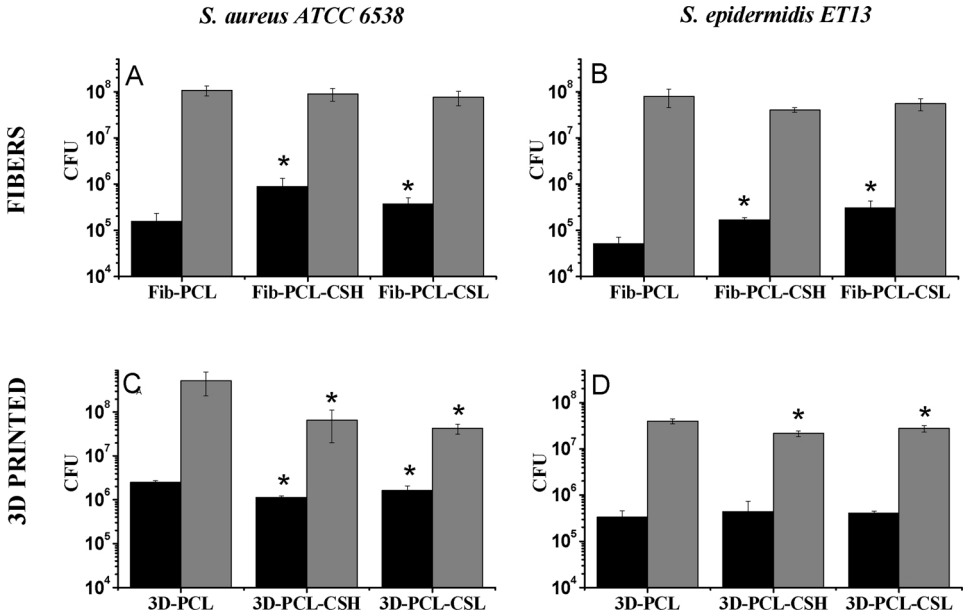

Fig. 6. Number of bacteria (colony forming units, CFU) recovered after 1 h adhesion (black) and after 24 h of biofilm formation (grey) with *S. aureus* ATCC 6538 (A, C) or *S. epidermidis* ET13 (B, D). Samples which are significantly different than the corresponding unmodified PCL scaffold under t-student test are marked with * ($p < 0.05$).

the Coomassie blue dye. As detailed in Fig. 3, native PCL scaffolds showed no coloration, while 3D-PCL-CSH presented a dark blue color, demonstrating the presence of chitosan on the structure, and 3D-PCL-CSL gave a light blue color due to the less effective coverage of the surface obtained with this chitosan. All these observations were in good correlation with the XPS analysis previously described.

3.4. Cytotoxicity evaluation of the scaffolds

To assess the cytotoxicity and cell hosting ability, the fabricated

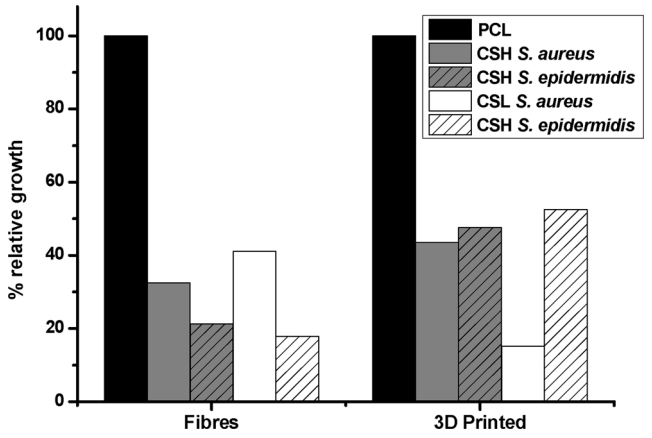

Fig. 7. Relative bacterial growth after 24 h with respect to PCL (black columns) for surfaces modified fibers and 3D printed scaffold with CSH (grey columns) and CSL (plain columns) tested against *S. aureus* ATCC 6538 (plain columns) and *S. epidermidis* ET 13 (striped columns).

scaffolds were evaluated in vitro. A lactate dehydrogenase (LDH) assay was used to measure the rate of cell death 24 h after seeding the cells on top of the scaffolds (Fig. 4). LDH is released from dying cells due to a loss of plasma membrane integrity. High levels of LDH indicate either cytotoxicity or cell death due to impaired cellular adhesion. The results obtained for all of the samples tested indicated high cell viability, suggesting high biological compatibility. Accordingly, it was concluded that the tested scaffolds were non-cytotoxic. These findings are in line with previous studies documenting the favorable biocompatibility of both PCL and chitosan based structures (Gorzelanny, Poppelmann, Pappelbaum, Moerschbacher, & Schneider, 2010; Kaiser, Chalapala, Gorzelanny, Perali, & Goycoolea, 2016), and confirmed that the surface modification process did not lead to any toxicity in the final samples.

Furthermore, reflecting the LDH results recorded after 24 h, L929 cells were detected on the scaffolds even after a more prolonged cultivation time of 7 days, confirming negligible cytotoxicity of the specimens. To cope with the three-dimensionality of the samples in terms of imaging, structured illumination fluorescence microscopy (SIFM) was used, which facilitated confocal-like imaging of the scaffolds (Gorzelanny et al., 2016). Although the dense fiber arrangement in the mats resulted in strong light scattering which interfered with microscopic imaging, a confluent cell population on all of the tested fiber mats samples could be identified (Fig. 5). Comparatively, less cells were found on the 3D-scaffolds, which is probably related to the larger corresponding growth area of the fiber mats. However, the spindle-like morphology of the cells and the strong staining of the actin cytoskeleton, in all cases, suggest a non-affected fibroblastic phenotype (Fig. 5) (Madathil, Damodaran, Thrikkovil, & Mohanty, 2012).

3.5. Evaluation of the antibacterial properties of the scaffolds

Chitosan was immobilized on the scaffold structures in order to provide it with enhanced antibacterial activity. Two different bacteria were used to evaluate the antimicrobial properties of the fabricated scaffolds, *S. aureus* ATCC 6538 and *S. epidermidis* ET13. The antibacterial properties of chitosan are strongly pH dependent, as previously reported in the literature (Rabea, Badawy, Stevens, Smagghe, & Steurbaut, 2003). In the present study, the pH was measured at the beginning and end of the antibacterial assays. At the starting point the pH was 7.5, and as the bacteria kept growing, the pH decreased to 7.3 after 1 h and down to 6.0 after 24 h. This drop in pH can be attributed to the production of acidic components associated with the bacterial metabolism (Vandecandelaere, Van Nieuwerburgh, Deforce, & Coenye, 2017). The antibacterial properties of chitosan are associated with the presence of deacetylated units due to amino protonation (pKa 6.2). The number of CFU (colony-forming units) recovered from each type of scaffold, after 1 h adhesion and 24 h biofilm formation are shown in Fig. 6. In the case of fiber mats the adhesion of both bacteria after 1 h was significantly higher for chitosan modified samples. Nevertheless, the number of CFU after 24 h was comparable for modified and unmodified fiber mats. For 3D printed structures, significant differences were observed between the control PCL scaffolds and the chitosan modified materials after 24 h for both bacteria. Therefore, although the surface modification seemed more efficient in the case of fiber mats, the impact of the antibacterial surface properties was more noticeable for 3D printed structures, as for fibers the high surface area leads to better bacteria adhesion (Fig. 6).

Moreover, the relative increase in the number of attached bacteria between 1 h and 24 h (Eq. (1)) was calculated. Translating this relative increase in relative growth in relation to the native PCL materials by using Eq. (2), the effect of the chitosan modification on surface colonization can be estimated (Fig. 7).

A clear reduction in the bacterial growth for the chitosan modified fibers and 3D printed scaffolds in comparison to native PCL can be observed (Fig. 7). For fiber mats, even though XPS data revealed more efficient immobilization of chitosan for CSH than for CSL, no difference was observed between both in regards to their antibacterial activity. For 3D printed structures, a more pronounce decrease in growth rate of *S. aureus* was detected for scaffolds modified with CSL.

4. Conclusions

Successful covalent chitosan coupling to PCL scaffolds was achieved by a two-step surface functionalization procedure. PCL scaffolds, in the shape of electrospun fiber mats and 3D printed structures, were surface modified by argon plasma treatment followed by novel NHSMA grafting and subsequently reacted with chitosan, of varying molecular weights. The relatively higher N% recorded for the fibers in XPS analysis indicates that the reaction was more successful for fibers than 3D printed materials. CSH which had the highest Mw, yielded the highest N/C ratio for both scaffold types indicative of better binding. Visualization of chitosan functionalization was realized through SEM for the electrospun mats and with Coomassie blue staining for the 3D printed scaffolds. The observations supported the conclusions taken from XPS analysis, with CSH providing the most homogeneous coverage on the PCL scaffolds. Additionally, the materials developed using CSH and CSL were shown to be non-cytotoxic and were conducive to fibroblast L929 adhesion and proliferation. Whereas surface modification is more efficient on fiber mats due to its larger surface area, it comes at the expense of a decrease in antibacterial properties in comparison with 3D printed structures as it leads to better bacteria adhesion. The scaffolds were neither bactericidal nor bacteriostatic, but the antibacterial activity of chitosan against *S. aureus* ATCC 6538 and *S. epidermidis* ET13 was evidently seen as a decrease in bacteria growth on the modified samples for both types of scaffolds regardless the chitosan molecular weight. Future works will focus on the study of different types of bacteria and possible inflammatory reaction upon implantation of the scaffolds.

Author contributions

The manuscript was written through contributions of all authors. All authors have given approval to the final version of the manuscript.

Conflicts of interest

There are no conflicts of interest to declare

Acknowledgments

The authors gratefully acknowledge support from the BOF grant DOZA/IL/DDC/GDG/DL/130b-2014 and the financial support of the

Nano3Bio EU project (Grant agreement n° 613931). Pol Agusti Cervia, a visiting Erasmus student assisted at the early stages of this work.

Appendix A. Supplementary data

Supplementary data associated with this article can be found, in the online version, at https://doi.org/10.1016/j.carbpol.2018.02.060.

References

Achilli, T.-M., Meyer, J., & Morgan, J. R. (2012). Advances in the formation, use and understanding of multi-cellular spheroids. *Expert Opinion on Biological Therapy, 12*(10), 1347–1360.

Anitha, A., Divya Rani, V. V., Krishna, R., Sreeja, V., Selvamurugan, N., Nair, S. V., ... Jayakumar, R. (2009). Synthesis, characterization, cytotoxicity and antibacterial studies of chitosan, O-carboxymethyl and N,O-carboxymethyl chitosan nanoparticles. *Carbohydrate Polymers, 78*(4), 672–677.

Bauer, A. T., Strozyk, E. A., Gorzelanny, C., Westerhausen, C., Desch, A., Schneider, M. F., & Schneider, S. W. (2011). Cytotoxicity of silica nanoparticles through exocytosis of von Willebrand factor and necrotic cell death in primary human endothelial cells. *Biomaterials, 32*(33), 8385–8393.

Bhardwaj, N., & Kundu, S. C. (2010). Electrospinning: A fascinating fiber fabrication technique. *Biotechnology Advances, 28*(3), 325–347.

Cai, Y., Li, J., Poh, C. K., Tan, H. C., San Thian, E., Fuh, J. Y. H., ... Wang, W. (2013). Collagen grafted 3D polycaprolactone scaffolds for enhanced cartilage regeneration. *Journal of Materials Chemistry B, 1*(43), 5971–5976.

Chen, S.-H., Chen, C.-H., Fong, Y. T., & Chen, J.-P. (2014). Prevention of peritendinous adhesions with electrospun chitosan-grafted polycaprolactone nanofibrous membranes. *Acta Biomaterialia, 10*(12), 4971–4982.

Cheng, Z., & Teoh, S.-H. (2004). Surface modification of ultra thin poly (ε-caprolactone) films using acrylic acid and collagen. *Biomaterials, 25*(11), 1991–2001.

Chia, H. N., & Wu, B. M. (2015). Recent advances in 3D printing of biomaterials. *Journal of Biological Engineering, 9*(1), 4.

Ciardelli, G., & Chiono, V. (2006). Materials for peripheral nerve regeneration. *Macromolecular Bioscience, 6*(1), 13–26.

Coombes, A., Rizzi, S., Williamson, M., Barralet, J., Downes, S., & Wallace, W. (2004). Precipitation casting of polycaprolactone for applications in tissue engineering and drug delivery. *Biomaterials, 25*(2), 315–325.

Cooper, A., Oldinski, R., Ma, H., Bryers, J. D., & Zhang, M. (2013). Chitosan-based nanofibrous membranes for antibacterial filter applications. *Carbohydrate Polymers, 92*(1), 254–259.

Deng, X., Nikiforov, A. Y., Coenye, T., Cools, P., Aziz, G., Morent, R., ... Leys, C. (2015). Antimicrobial nano-silver non-woven polyethylene terephthalate fabric via an atmospheric pressure plasma deposition process. *Scientific Reports, 5*, 10138.

Desmet, T., Morent, R., De Geyter, N., Leys, C., Schacht, E., & Dubruel, P. (2009). Nonthermal plasma technology as a versatile strategy for polymeric biomaterials surface modification: A review. *Biomacromolecules, 10*(9), 2351–2378.

Desmet, T., Billiet, T., Berneel, E., Cornelissen, R., Schaubroeck, D., Schacht, E., & Dubruel, P. (2010). Post-plasma grafting of AEMA as a versatile tool to biofunctionalise polyesters for tissue engineering. *Macromolecular Bioscience, 10*(12), 1484–1494.

Desmet, T., Poleunis, C., Delcorte, A., & Dubruel, P. (2012). Double protein functionalized poly-epsilon-caprolactone surfaces: In depth ToF-SIMS and XPS characterization. *Journal of Materials Science-Materials in Medicine, 23*(2), 293–305.

Doulabi, A. H., Mirzadeh, H., Imani, M., & Samadi, N. (2013). Chitosan/polyethylene glycol fumarate blend film: Physical and antibacterial properties. *Carbohydrate Polymers, 92*(1), 48–56.

Feng, Y., & Xia, W. (2011). Preparation, characterization and antibacterial activity of water-soluble O-fumaryl-chitosan. *Carbohydrate Polymers, 83*(3), 1169–1173.

Ghorbani, F. M., Kaffashi, B., Shokrollahi, P., Seyedjafari, E., & Ardeshirylajimi, A. (2015). PCL/chitosan/Zn-doped nHA electrospun nanocomposite scaffold promotes adipose derived stem cells adhesion and proliferation. *Carbohydrate Polymers, 118*, 133–142.

Gorzelanny, C., Poppelmann, B., Pappelbaum, K., Moerschbacher, B. M., & Schneider, S. W. (2010). Human macrophage activation triggered by chitotriosidase-mediated chitin and chitosan degradation. *Biomaterials, 31*(33), 8556–8563.

Gorzelanny, C., Kmeth, R., Obermeier, A., Bauer, A. T., Halter, N., Kumpel, K., ... Schneider, S. W. (2016). Silver nanoparticle-enriched diamond-like carbon implant modification as a mammalian cell compatible surface with antimicrobial properties. *Scientific Reports, 6*, 22849.

Ho, M. H., Hou, L. T., Tu, C. Y., Hsieh, H. J., Lai, J. Y., Chen, W. J., & Wang, D. M. (2006). Promotion of cell affinity of porous PLLA scaffolds by immobilization of RGD peptides via plasma treatment. *Macromolecular Bioscience, 6*(1), 90–98.

Hockaday, L., Kang, K., Colangelo, N., Cheung, P., Duan, B., Malone, E., ... Lipson, H. (2012). Rapid 3D printing of anatomically accurate and mechanically heterogeneous aortic valve hydrogel scaffolds. *Biofabrication, 4*(3), 035005.

Hollister, S. J. (2005). Porous scaffold design for tissue engineering. *Nature Materials, 4*(7), 518–524.

Hong, S., & Kim, G. (2011). Fabrication of electrospun polycaprolactone biocomposites reinforced with chitosan for the proliferation of mesenchymal stem cells. *Carbohydrate Polymers, 83*(2), 940–946.

Hutmacher, D. W., Schantz, T., Zein, I., Ng, K. W., Teoh, S. H., & Tan, K. C. (2001). Mechanical properties and cell cultural response of polycaprolactone scaffolds designed and fabricated via fused deposition modeling. *Journal of Biomedical Materials Research, 55*(2), 203–216.

Ji, Y., Liang, K., Shen, X., & Bowlin, G. L. (2014). Electrospinning and characterization of chitin nanofibril/polycaprolactone nanocomposite fiber mats. *Carbohydrate Polymers, 101*, 68–74.

Kaiser, M., Chalapala, S., Gorzelanny, C., Perali, R. S., & Goycoolea, F. M. (2016). The effect of capsaicin derivatives on tight-junction integrity and permeability of Madin-Darby canine kidney cells. *Journal of Pharmaceutical Sciences, 105*(2), 630–638.

Lee, J. Y., Lee, J.-W., & Schmidt, C. E. (2008). Neuroactive conducting scaffolds: Nerve growth factor conjugation on active ester-functionalized polypyrrole. *Journal of the Royal Society Interface* rsif. 2008.0403.

Li, W.-J., Tuli, R., Okafor, C., Derfoul, A., Danielson, K. G., Hall, D. J., & Tuan, R. S. (2005). A three-dimensional nanofibrous scaffold for cartilage tissue engineering using human mesenchymal stem cells. *Biomaterials, 26*(6), 599–609.

Madathil, B. K., Damodaran, V., Thrikkovil, K. V., & Mohanty, M. (2012). F-actin and alpha-actinin reorganization mediates initial fibroblast interaction with CoCr alloy particles in vitro. *Microscopy Research and Technique, 75*(11), 1539–1549.

Mahoney, C., Conklin, D., Waterman, J., Sankar, J., & Bhattarai, N. (2016). Electrospun nanofibers of poly (ε-caprolactone)/depolymerized chitosan for respiratory tissue engineering applications. *Journal of Biomaterials Science, Polymer Edition,* 1–21 (just-accepted).

Martins, A. F., Facchi, S. P., Follmann, H. D., Pereira, A. G., Rubira, A. F., & Muniz, E. C. (2014). Antimicrobial activity of chitosan derivatives containing N-quaternized moieties in its backbone: A review. *International Journal of Molecular Sciences, 15*(11), 20800–20832.

Mendes, A. C., Gorzelanny, C., Halter, N., Schneider, S. W., & Chronakis, I. S. (2016). Hybrid electrospun chitosan-phospholipids nanofibers for transdermal drug delivery. *International Journal of Pharmaceutics, 510*(1), 48–56.

Morent, R., De Geyter, N., Desmet, T., Dubruel, P., & Leys, C. (2011). Plasma surface modification of biodegradable polymers: A review. *Plasma Processes and Polymers, 8*(3), 171–190.

Muzzarelli, R., Tarsi, R., Filippini, O., Giovanetti, E., Biagini, G., & Varaldo, P. (1990). Antimicrobial properties of N-carboxybutyl chitosan. *Antimicrobial Agents and Chemotherapy, 34*(10), 2019–2023.

Nourmohammadi, J., Ghaee, A., & Liavali, S. H. (2016). Preparation and characterization of bioactive composite scaffolds from polycaprolactone nanofibers-chitosan-oxidized starch for bone regeneration. *Carbohydrate Polymers, 138*, 172–179.

Peltola, S. M., Melchels, F. P., Grijpma, D. W., & Kellomäki, M. (2008). A review of rapid prototyping techniques for tissue engineering purposes. *Annals of Medicine, 40*(4), 268–280.

Pham, Q. P., Sharma, U., & Mikos, A. G. (2006). Electrospinning of polymeric nanofibers for tissue engineering applications: A review. *Tissue Engineering, 12*(5), 1197–1211.

Rabea, E. I., Badawy, M. E.-T., Stevens, C. V., Smagghe, G., & Steurbaut, W. (2003). Chitosan as antimicrobial agent: Applications and mode of action. *Biomacromolecules, 4*(6), 1457–1465.

Sarasam, A., & Madihally, S. V. (2005). Characterization of chitosan–polycaprolactone blends for tissue engineering applications. *Biomaterials, 26*(27), 5500–5508.

Si, J., Cui, Z., Wang, Q., Liu, Q., & Liu, C. (2016). Biomimetic composite scaffolds based on mineralization of hydroxyapatite on electrospun poly (ε-caprolactone)/nanocellulose fibers. *Carbohydrate Polymers, 143*, 270–278.

Siri, S., Wadbua, P., Amornkitbamrung, V., Kampa, N., & Maensiri, S. (2010). Surface modification of electrospun PCL scaffolds by plasma treatment and addition of adhesive protein to promote fibroblast cell adhesion. *Materials Science and Technology, 26*(11), 1292–1297.

Sousa, I., Mendes, A., Pereira, R. F., & Bártolo, P. J. (2014). Collagen surface modified poly (ε-caprolactone) scaffolds with improved hydrophilicity and cell adhesion properties. *Materials Letters, 134*, 263–267.

Suzuki, M., Kishida, A., Iwata, H., & Ikada, Y. (1986). Graft copolymerization of acrylamide onto a polyethylene surface pretreated with glow discharge. *Macromolecules, 19*(7), 1804–1808.

Tan, L., Hu, J., Huang, H., Han, J., & Hu, H. (2015). Study of multi-functional electrospun composite nanofibrous mats for smart wound healing. *International Journal of Biological Macromolecules, 79*, 469–476.

Vandecandelaere, I., Van Nieuwerburgh, F., Deforce, D., & Coenye, T. (2017). Metabolic activity, urease production, antibiotic resistance and virulence in dual species biofilms of Staphylococcus epidermidis and *Staphylococcus aureus*. *Plos One, 12*(3), e0172700.

Wang, C., Yan, Q., Liu, H.-B., Zhou, X.-H., & Xiao, S.-J. (2011). Different EDC/NHS activation mechanisms between PAA and PMAA brushes and the following amidation reactions. *Langmuir, 27*(19), 12058–12068.

Woodruff, M. A., & Hutmacher, D. W. (2010). The return of a forgotten polymer—Polycaprolactone in the 21st century. *Progress in Polymer Science, 35*(10), 1217–1256.

Worthington, P., Pochan, D. J., & Langhans, S. A. (2015). Peptide hydrogels?versatile matrices for 3D cell culture in cancer medicine. *Frontiers in Oncology, 5*.

Yang, S., Leong, K.-F., Du, Z., & Chua, C.-K. (2001). The design of scaffolds for use in tissue engineering. Part I. Traditional factors. *Tissue Engineering, 7*(6), 679–689.

Yang, S., Leong, K.-F., Du, Z., & Chua, C.-K. (2002). The design of scaffolds for use in tissue engineering. Part II. Rapid prototyping techniques. *Tissue Engineering, 8*(1), 1–11.

Yen, K.-C., Chen, C.-Y., Huang, J.-Y., Kuo, W.-T., & Lin, F.-H. (2016). Fabrication of keratin/fibroin membranes by electrospinning for vascular tissue engineering. *Journal of Materials Chemistry B, 4*(2), 237–244.

Yuan, S., Xiong, G., Wang, X., Zhang, S., & Choong, C. (2012). Surface modification of polycaprolactone substrates using collagen-conjugated poly (methacrylic acid) brushes for the regulation of cell proliferation and endothelialisation. *Journal of Materials Chemistry, 22*(26), 13039–13049.

Zhu, Y., Gao, C., Liu, X., & Shen, J. (2002). Surface modification of polycaprolactone membrane via aminolysis and biomacromolecule immobilization for promoting cytocompatibility of human endothelial cells. *Biomacromolecules, 3*(6), 1312–1319.